Measurement of liquid film thickness in a micro parallel channel with interferometer and laser focus displacement meter

Youngbae Han, Naoki Shikazono and Nobuhide Kasagi

Department of Mechanical Engineering, The University of Tokyo
Hongo 7-3-1, Bunkyo-ku, Tokyo 113-8656, Japan
Tel: +81-3-5452-6777; Fax: +81-3-5452-6777

Email address: ybhan@iis.u-tokyo.ac.jp (Youngbae Han),
shika@iis.u-tokyo.ac.jp (Naoki Shikazono),
kasagi@thtlab.t.u-tokyo.ac.jp (Nobuhide Kasagi).

Abstract

In the present study, liquid film thicknesses in parallel channels with heights of H = 0.1, 0.3 and 0.5 mm are measured with two different optical methods, i.e., interferometer and laser focus displacement meter. Ethanol is used as a working fluid. Liquid film thicknesses obtained from two optical methods agree very well. At low capillary numbers, dimensionless liquid film thickness is in accordance with Taylor's law. However, as capillary number increases, dimensionless liquid film thickness becomes larger than Taylor's law for larger channel heights. It is attributed to the dominant inertial effect at high capillary numbers. Using channel height H for dimensionless liquid film thickness δ_0/H and hydraulic diameter $D_h = 2H$ as the characteristic length for Reynolds and Weber numbers, liquid film thickness in a parallel channels can be predicted well by the circular tube correlation proposed by Han and Shikazono (2009a). This is because curvature differences between bubble nose and flat film region are identical in circular tubes and parallel channels.

1. Introduction

In recent years, two-phase flow in micro channels has been investigated extensively because of its superior heat and mass transfer characteristics. Flow regime is an important parameter to determine two-phase flow characteristics, i.e., heat transfer, pressure drop, chemical reaction and so on. The effect of surface tension on flow regimes becomes larger in micro channels (Cheng et al., 2008). Bubble occupies the whole cross section of the channel and develops as an elongated bubble. This flow regime is called slug flow. Slug flow is one of the main flow regimes in micro channels. In slug flow, thin liquid film between channel wall and vapor bubble plays an important role in heat and mass transfer.

Liquid film formation is strongly affected by channel geometries, e.g., circular, rectangular, triangular etc. Thus, the effect of channel geometry on the liquid film has been investigated by many research groups using circular and square channels under adiabatic condition (Thulasidas et al., 1995; Bi and Zhao, 2001; Chung et al., 2004; Han and Shikazono, 2009a, b). It was observed that bubble in a square channel was not axisymetric at small capillary numbers.

Compared to circular and square channels, experimental researches on the two-phase flow in a micro parallel channel have been conducted by very few research groups. Moriyama and Inoue (1996) measured the liquid film thickness between two parallel plates with narrow gaps, H = 0.1, 0.2 and 0.4 mm. In their experiment, liquid film was formed by vapor bubble expansion. They measured time variation of wall temperature. Liquid film thickness was calculated assuming that heat was solely consumed by liquid film evaporation. Experimental correlation was proposed in terms of capillary number and Bond number defined by the interface acceleration.

Utaka et al. (2007) used laser extinction method to measure the liquid film thickness in narrow channels. Channel heights employed in their experiments were H = 0.15, 0.3 and 0.5 mm. Liquid film thickness increased linearly with bubble velocity and became constant at bubble velocity above approximately 2 m/s. Boiling in narrow channels was characterized by the micro-layer dominant and the saturated liquid periods.

It is reported that liquid film thickness in slug flow is mainly determined by the balance between viscous and surface tension forces (Bretherton, 1961). Inertial force is usually neglected in micro-scale two-phase flow. However, it is observed that inertial force has a large effect on the liquid film thickness even in micro scales as capillary number increases (Han and Shikazono, 2009a). The effect of inertial force on the liquid film thickness is not clear when the channel geometry is changed. For example, liquid film thickness can be scaled by tube diameter or channel height according to geometrical constraint, but inertia effect is usually expressed by hydraulic diameter which becomes twice of channel height in case of parallel channels. This must be investigated for liquid film thickness prediction. In addition, there's no evidence for instantaneous liquid film to be uniform in spanwise direction in a parallel channel. To investigate the two dimensionality of the flow field, interferometer is introduced to measure instantaneous spanwise liquid film profiles.

In the present study, liquid film thickness in a micro parallel channel is measured under adiabatic condition by two optical methods, i.e., laser focus displacement meter and interferometer, and the effect of inertial force on the liquid film thickness is investigated. The results obtained by those two methods are compared with each other. Measured liquid film thickness is also compared with the circular tube results of Han and Shikazono (2009a). The similarity between liquid film thicknesses in micro circular and parallel channels is discussed.

2. Experimental setup and procedures

2.1. Experimental setup

Figure 1 shows the schematic diagram of the experimental setup. Rectangular channels with large aspect ratio (Japan Cell©) made of quartz are used as test channels. Three rectangular channels are employed in the present study. Channel heights are H = 0.1, 0.3 and 0.5 mm. Channel heights at several positions are measured with laser focus displacement meter, and averaged values are used. Variations of measured heights were less than 2% for all rectangular channels. Widths of rectangular channels are W = 4, 7 and 10 mm for H = 0.1, 0.3 and 0.5 mm channels, respectively. Aspect ratios are larger

than approximately W/H = 20 for all channels. Thus, the flow at the center of the channel span is almost identical to the flow in parallel channels. Table 1 shows the dimensions of rectangular channels used in this study. Aluminum block and Swagelok© union are used to connect the test channel to the experimental setup as shown in Fig. 2.

In Fig. 1, one end of the test channel is connected to the syringe and the actuator motor (EZHC6A-101, Oriental Motor). The other end of the test channel is open to air. Actuator motor is employed to move the working fluid in the test channel. Syringes (1700 series, Hamilton) with several cross sectional areas are employed to control the liquid velocity in the test channel. Ethanol is used as a working fluid. Interferometer (Mizojiri Optical Company) and laser focus displacement meter (hereafter LFDM; LT9010M, Keyence) are employed to measure the liquid film thickness. Fringe patterns caused by liquid film profile are obtained with interferometer. High-speed camera (SA1.1, Photron) is used to capture the fringe pattern images. Liquid film thickness measured by LFDM is transformed to DC voltage signal in the range of ±10 V. Output signal was sent to PC through GPIB interface and recorded with LabVIEW.

2.2 Experimental procedures

Ethanol is injected into the syringe and the piston of syringe is connected to the actuator motor. After the inner wall of test channel is purged with pressurized dry air for several minutes, the test channel is connected to the syringe. Working fluid is moved by the actuator motor until the air-liquid interface is located near the open end of the test channel. Then, working fluid is pulled by the actuator motor and liquid film is formed on the wall. The movement of air-liquid interface is captured by the high-speed camera. Images are taken at several frame rates according to the interface velocity. For the maximum interface velocity, frame rate is 5000 frames per second. Velocity profile along the flow direction is calculated from the captured images. In the case of LFDM, liquid film thickness is measured simultaneously with the high-speed camera. In the case of interferometer, high-speed camera is used to measure both fringe patterns and bubble velocity. Thus, bubble velocity and liquid film thickness are measured at different test runs. Fringe pattern images are captured at the frame rate of 1000 frames per second.

2.3 Principles of measurement methods

2.3.1 Interferometer

Several researchers have used interferometer to measure the liquid film thickness (Nozhat, 1997; Sashidhar et al., 2006). Figure 3 shows the schematic diagram of the interferometer and an example of the captured fringe pattern image. Reflected light from the inner wall surface and the air-liquid interface interferes and makes fringe patterns corresponding to the liquid film thickness. When twice of liquid film thickness becomes even multiple of half laser wavelength divided by refractive index of the liquid, reflected light makes constructive interference and white fringe appears. On the other hand, black fringe appears for odd multiples. The relation between liquid film thickness and interference fringes can be expressed as follows:

$$\delta = (2m+1)\frac{\lambda_{\text{laser}}}{4n_{\text{L}}}, \quad (\text{Destructive interference}) \tag{1}$$

$$\delta = 2m\frac{\lambda_{\text{laser}}}{4n_{\text{L}}}, \quad (\text{Constructive interference}) \tag{2}$$

where m is the number of fringes, λ is the wavelength of laser and n_{L} is the refractive index of the working fluid. Refractive index of ethanol is 1.36. In the present interferometer, He-Ne laser is used and the wavelength λ_{laser} is 632.8 nm. If the angle of target surface is larger than 2°, reflected light is not detected by interferometer. Thus, fringe pattern image close to the bubble nose cannot be obtained.

At the initial interface position, fringe pattern does not appear because contact angle is beyond the measurement angle limit of interferometer. Liquid film is then formed on the wall as the interface is pulled by the actuator motor. The liquid film profile along the flow direction can be obtained from the fringe pattern image captured by high-speed camera. Figure 4 shows an example of liquid film profile obtained from the fringe pattern image. In Fig. 4 (a), liquid film thickness is zero at the initial interface position.

The position of test channel is adjusted in advance so that it is placed in parallel with the interferometer using XYZ stage and θαβ angular stage. The size of fringe pattern image is 0.88 mm × 0.66 mm. Due to the limitation of image size, fringe patterns need to be captured at several positions along the flow direction as shown in Fig. 5. Each fringe pattern image is captured at different test runs, but it is confirmed that nearly identical flow is reproduced at different test runs. Figure 6 shows velocity variations along the flow direction for different test runs. Almost identical velocity profiles are obtained as shown in Fig. 6.

Figure 7 shows the time variation of the fringe pattern at the first measurement position, z = 0 - 660 μm shown in Fig. 5. Working fluid is ethanol and channel height is 0.3 mm. At t = 0 ms, there is no fringe pattern visible because the test channel is filled with liquid. As the air-liquid interface moves down, liquid film is formed on the channel wall and fringe pattern appears. At t = 6 ms, liquid film is formed on the whole imaging area. Figure 8 shows the time variation of liquid film profile obtained from the fringe pattern images in Fig. 7. Fringe pattern remains nearly unchanged against time. The number of fringes is counted after the fringe pattern covered whole imaging area. It should be noted that fringe pattern is straight and parallel in spanwise direction. Thus, instantaneous liquid film profile can be considered as two-dimensional.

Figure 9 shows the captured fringe pattern images at different measurement positions along the flow direction. Working fluid is ethanol and channel height is 0.3 mm. In Fig. 9, fringes are quite dense at the first position, z = 0 - 660 μm. Fringe density decreases along the flow direction, and fringe pattern finally disappears at the sixth position, z = 3300 - 3960 μm, where liquid film thickness becomes uniform. Figure 10 shows the liquid film profile obtained from the fringe pattern images in Fig. 9. Interface velocity is also plotted in Fig. 10 along the flow direction. Liquid film thickness increases with interface velocity.

2.3.2 Laser focus displacement meter

Laser focus displacement meter has been used by several researchers for the liquid film

thickness measurement (Takamasa and Kobayashi, 2000; Hazuku et al., 2005; Han and Shikazono, 2009a, b). On the principle and uncertainty analysis of LFDM, refer to the authors' previous paper (Han and Shikazono, 2009a). Laser path in the test channel wall is shown in Fig. 11. Liquid film thickness δ is calculated as follows:

$$\delta = \frac{H - y_{\mathrm{m}}}{2}, \tag{3}$$

where H is the channel height and y_{m} is the measured value as the movement of objective lens.

Figure 12 shows a typical measurement example of liquid film thickness. Time variation of the liquid film thickness at a fixed position is obtained by LFDM. If the angle of interface is larger than about 11°, intensity of the reflected light becomes weak and the interface position cannot be detected. Therefore, it is impossible to measure the whole shape of the bubble nose. Liquid film thickness only in the transition region and the flat film region can be measured. Initial decrease in Fig. 12 is the transition region between the bubble nose and the flat film region. After quick decrease, liquid film thickness is almost constant for some time. The liquid film thickness after the rapid decrease is defined as the initial liquid film thickness δ_0 as shown in Fig. 12. Initial liquid film thickness δ_0 is used for experimental data. As time passes further, liquid film eventually drains.

3. Experimental results and discussion

3.1 Comparison of liquid film thicknesses obtained by interferometer and LFDM

Three-dimensional shape of the liquid film can be obtained from the fringe pattern images. On the other hand, LFDM can only detect the liquid film thickness at one fixed measurement position. Figure 13 shows liquid film thicknesses obtained by interferometer versus interface velocity variations along the flow direction. Channel height is H = 0.5 mm. Liquid film thickness increases rapidly near to the starting position and then increases gradually with increasing interface velocity.

Figure 14 shows the liquid film thicknesses obtained by interferometer and LFDM. In the case of interferometer, liquid film thickness is calculated by accumulation of the number of fringes in each fringe pattern image along the flow direction. In Fig. 14, liquid film thickness and interface velocity at the most downstream position are plotted. When counting the number of fringes between neighboring images, it may have ±1 fringe error. As the number of images increases to count the total number of fringes, measurement error also increases. In Fig. 14, error bars on the interferometer data indicate uncertainty of 95 % confidence.

In the case of LFDM, it was reported that LFDM could measure liquid film thickness in a micro tube very accurately within 1% error (Hazuku et al., 2005). Curvature of micro tube wall is the main reason for measurement error. However, curvature problem disappears in micro parallel channels. Thus, measurement error in a micro parallel channel is smaller than that in a micro circular tube.

Interface velocity is obtained from the displacement of interface position between two captured images. Interface position has approximately ±2 pixels error in each captured image. Thus, the error in the displacement of interface position is ±4 pixels. In the present experiment, the displacement of interface position is approximately 100 pixels. Interface velocity error are shown as horizontal bars in Fig. 14. In Fig. 14, it is confirmed that both methods are effective to measure the liquid film thickness at moderate velocities.

Bretherton (1961) theoretically investigated liquid film thickness in slug flow with lubrication equations. It is reported that liquid film thickness increases in proportion to $Ca^{2/3}$, where Ca ($\mu U/\sigma$), μ, U and σ are capillary number, liquid viscosity, air-liquid interface velocity and surface tension, respectively. Aussillous and Quere (2000) proposed experimental correlation for the liquid film thickness in a circular mini tube, which is the curve fitting of the experimental results obtained by Taylor (1961) as follows:

$$\frac{\delta}{D} = \frac{0.67Ca^{2/3}}{1 + 3.35Ca^{2/3}}, \tag{4}$$

where δ is liquid film thickness and D is tube diameter. Equation (4) is called Taylor's law. Figure 15 shows the dimensionless liquid film thicknesses δ_0/H versus capillary number $Ca = \mu U/\sigma$ for the same experimental data in Fig. 14. At low capillary numbers, all experimental data are in good accordance with Taylor's law and liquid film thickness is determined only by the capillary number. However, as capillary number increases, liquid film thickness deviates from Taylor's law and liquid film thickness becomes larger for larger channels. This is attributed to the inertial force effect. At low capillary numbers, inertial force can be usually neglected. However, inertial force does affect liquid film formation as shown in Fig. 15. It is reported in Han and Shikazono (2009a) that, at relatively high capillary numbers, liquid film thickness in a micro circular tube initially decreases with Reynolds number and then increases after taking a minimum value.

3.2 Comparison with the liquid film thickness correlation for micro circular tube

Han and Shikazono (2009a) proposed an experimental correlation for the initial liquid film thickness in a micro circular tube as follows:

$$\frac{\delta_0}{D} = \frac{0.670Ca^{2/3}}{1 + 3.13Ca^{2/3} + 0.504Ca^{0.672}Re^{0.589} - 0.352We^{0.629}} \quad \left(Re < Re_{\mathrm{crit}}\right), \tag{5}$$

where δ_0, ρ and σ are initial liquid film thickness, liquid density and surface tension, respectively. Capillary, Reynolds and Weber numbers are defined as $Ca = \mu U/\sigma$, $Re = \rho UD/\mu$ and $We = \rho U^2 D/\sigma$. Equation (5) is valid only for steady laminar flow and liquid film thickness becomes constant for turbulent flow. Re_{crit} is the Reynolds number at which liquid flow changes from laminar to turbulent. In Han and Shikazono (2009a), $Re_{\mathrm{crit}} = 2000$ was used. Figure 16 shows the schematic diagram of the liquid film profile near to the bubble nose taken from Han and Shikazono (2009a). Momentum balance and curvature matching between the bubble nose and the transition region are expressed as follows:

$$\frac{\mu U}{\delta_0^2} \sim \frac{1}{\lambda}\left\{\sigma\left(\frac{2}{R-\delta_0}-\frac{1}{R-\delta_0}\right)\left(1+f\left(Re,Ca\right)\right)\right\}-\frac{1}{\lambda}\rho U^2, \tag{6}$$

$$\frac{\delta_0}{\lambda^2} \sim \left\{\frac{1}{R-\delta_0}\left(1+f\left(Re,Ca\right)\right)\right\}, \tag{7}$$

where λ is transition region length and $f(Re,Ca)$ represents the effects of Reynolds and capillary numbers on bubble nose curvature. Basic functional form of Eq. (5) is derived from Eqs. (6) and (7). This scaling analysis can be applied in the same manner for the parallel channels. In a circular tube, the curvature at bubble nose is $2/(R\text{-}\delta_0)$ and the curvature at flat film region is $1/(R\text{-}\delta_0)$. Therefore, curvature difference between these two regions is $1/(R\text{-}\delta_0)$ as shown in Eq. (6). In a parallel channel, the curvature at bubble nose is $1/(H/2\text{-}\delta_0)$ and that at flat film region is zero due to the flat wall. Although the curvatures at bubble nose and flat film region are different in circular tubes and parallel channels, the curvature differences become identical if R is replaced with $H/2$. Therefore, momentum and curvature matching equation in a parallel channel take the same form as Eqs. (6) and (7):

$$\frac{\mu U}{\delta_0^2} \sim \frac{1}{\lambda}\left\{\frac{\sigma}{H/2-\delta_0}\left(1+f\left(Re,Ca\right)\right)\right\}-\frac{1}{\lambda}\rho U^2, \tag{8}$$

$$\frac{\delta_0}{\lambda^2} \sim \left\{\frac{1}{H/2-\delta_0}\left(1+f\left(Re,Ca\right)\right)\right\}. \tag{9}$$

This supports the idea that the liquid film thickness correlation in a parallel channel also takes the same form as Eq. (5):

$$\frac{\delta_0}{H}=\frac{0.670Ca^{2/3}}{1+3.13Ca^{2/3}+0.504Ca^{0.672}Re^{0.589}-0.352We^{0.629}} \quad \left(Re<Re_{\text{critical}}\right). \tag{10}$$

Note that liquid film thickness is non-dimensionalized by channel height H. In general, inertial force effect is treated by Reynolds or Weber numbers using hydraulic diameter D_h. For example, laminar to turbulent transition of ducts with various cross-sectional shapes can be scaled quite well by Reynolds number based on hydraulic diameter

(Schlichting, 1979). Figure 17 shows dimensionless liquid film thickness versus hydraulic diameter at different capillary numbers. At small capillary numbers, liquid film thickness is almost constant, which means that liquid film thickness is independent of Reynolds number. At larger capillary numbers, liquid film thickness increases with hydraulic diameter. As shown in Fig. 17, dimensionless liquid film thickness can be scaled well by Reynolds number based on hydraulic diameter.

Figure 18 shows the dimensionless liquid film thickness in H = 0.5 mm parallel channel and in D = 1.0 mm circular tube, both having the same hydraulic diameter of D_h = 1.0 mm. Two experimental data show excellent agreement. This result also supports that Eq. (10) can be used also for the liquid film thickness in micro parallel channels if hydraulic diameter $D_h = 2H$ is used for Reynolds and Weber numbers. Figure 19 shows the comparison between experimental data and prediction value with Eq. (10) using hydraulic diameter as the characteristic length for Reynolds and Weber numbers, i.e., $Re = \rho U(2H)/\mu$ and $We = \rho U^2(2H)/\sigma$. Equation (10) can predict liquid film thickness remarkably well.

Liquid film profile is also predicted from interface velocity profile using Eq. (10). Figure 20 shows the comparison between the liquid film profile obtained with interferometer and the predicted liquid film profile from interface velocity profile. In the present experiment, interface velocity is not constant and accelerated even at the most downstream measurement position. The effect of acceleration on the liquid film thickness was investigated by Han and Shikazono (2010). It is reported that liquid film thickness is not affected if acceleration is small. The interface acceleration in the present study is smaller than the criteria shown in Han and Shikazono (2010). Thus, acceleration effect is considered to be negligible in the present experiment. In Fig. 20, Eq. (10) can also predict liquid film profile relatively well.

However, liquid film thickness is overestimated very close to the initial interface position as shown in Fig. 21. In the parallel channel of H = 0.5 mm, prediction is much larger than the experimental data at $z < 200$ μm. As channel height decreases, difference becomes smaller. Initial air-liquid interface in a micro parallel channel is nealy semicircle with diameter of H. It is considered that liquid flow close to the initial

interface is different from that in the region filled with liquid. Except very near to the dry wall, Eq. (10) is also applicable to the liquid film thickness in a micro parallel channel.

4. Conclusions

In the present study, liquid film thickness in a micro parallel channel is measured by two different optical methods, i.e., interferometer and laser focus displacement meter. It is confirmed from the interferometer measurement that instantaneous spatial variation of the liquid film profile in parallel channel can be neglected. In addition, liquid film thicknesses measured by two methods agreed very well. At small capillary numbers, dimensionless liquid film thickness follows Taylor's law and liquid film thickness is determined only by capillary number. As capillary number increases, dimensionless liquid film thickness deviates from Taylor's law and shows larger value for larger channels. This is attributed to the dominant inertial effect at high capillary numbers. Experimental correlation for the initial liquid film thickness in micro circular tubes proposed by Han and Shikazono (2009a) can predict the liquid film thickness in a micro parallel channel very well if hydraulic diameter $D_h = 2H$ is used for Reynolds and Weber numbers. This is because the force balance that dominates liquid film formation is similar in both circular tube and parallel channel.

Acknowledgement

We would like to thank Prof. Suzuki and Dr. Hasegawa for the fruitful discussions and suggestions. This work is supported through Grant in Aid for Scientific Research (No. 20560179) by MEXT, Japan and also the GCOE program "Mechanical Systems Innovation" by MEXT, Japan.

References

Aussillous, P. and Quere, D., 2000, "Quick deposition of a fluid on the wall of a tube," Phys. Fluids, 12, pp. 2367-2371.

Bi, Q. C. and Zhao, T. S., 2001, "Taylor bubbles in miniaturized circular and

noncircular channels," Int. J. Multiphase Flow, 27, pp. 561-570.

Bretherton, F. P., 1961, "The motion of long bubbles in tubes," J. Fluid Mech., 10, pp. 166-188.

Cheng, L., Ribatski, G. and Thome, J. R., 2008, "Two-phase flow patterns and flow-pattern maps: fundamentals and applications," Applied Mechanics Reviews, 61, pp. 050802-1-28

Chung, P. M. –Y., Kawaji M., Kawahara, A. and Shibata, Y., 2004, "Two-phase flow through square and circular microchannels – Effects of channel geometry," J. Fluid Eng. ASME, 126, pp. 546-552.

Han, Y. and Shikazono, N., 2009a, "Measurement of the liquid film thickness in micro tube slug flow," Int. J. Heat Fluid Flow. 35, pp. 896-903.

Han, Y. and Shikazono, N., 2009b, "Measurement of liquid film thickness in micro square channel," Int. J. Multiphase Flow, 30, pp. 842-853.

Han, Y. and Shikazono, N., 2010, "The effect of bubble acceleration on the liquid film thickness in micro tubes," Int. J. Heat Fluid Flow, 31, pp. 630-639.

Hazuku, T., Fukamachi, N., Takamasa, T., Hibiki, T. and Ishii, M., 2005, "Measurement of liquid film in microchannels using a laser focus displacement meter," Exp. in Fluids, 38, pp. 780-788.

Moriyama, K. and Inoue, A., 1996, "Thickness of the liquid film formed by a growing bubble in a narrow gap between two horizontal plates," J. Heat Transfer ASME, 118, pp. 132-139.

Nozhat, W. M., 1997, "Measurement of liquid-film thickness by laser interferometry," Appl. Opt., 36, pp. 7864-7869.

Sashidhar, S. P., Plawsky, J. L. and Wayner, P. C., 2006, “Microscale heat transfer in an evaporating moving extended meniscus,” Exp. Therm. Fluid Sci., 30, pp. 745-754.

Schlichting, H., 1979, “Boundary layer theory 7th ed.” McGraw-Hill, pp. 612-613.

Takamasa, T. and Kobayashi, K., 2000, “Measuring interfacial waves on film flowing down tube inner wall using laser focus displacement meter,” J. Multiphase Flow, 26, pp. 1493-1507.

Taylor, G. I., 1961, “Deposition of a viscous fluid on the wall of a tube,” J. Fluid Mech., 10, pp. 161-165.

Thulasidas, T. C., Abraham, M. A. and Cerro, R. L., 1995, “Bubble-train flow in capillaries of circular and square cross section,” Chem. Eng. Sci., 50, pp. 183-199.

Utaka, Y., Okuda, S. and Tasaki, Y., 2007, “Structure of micro-layer and characteristics of boiling heat transfer in narrow gap mini-channel system,” Trans. of the JSME Series B, 73, 1929-1935.

Table 1: Dimensions of the rectangular channels

Height H (mm)	Width W (mm)	Aspect ratio W/H	Length L (mm)
0.116	4.0	34.5	80.0
0.309	7.0	22.7	80.0
0.504	10.0	19.8	80.0

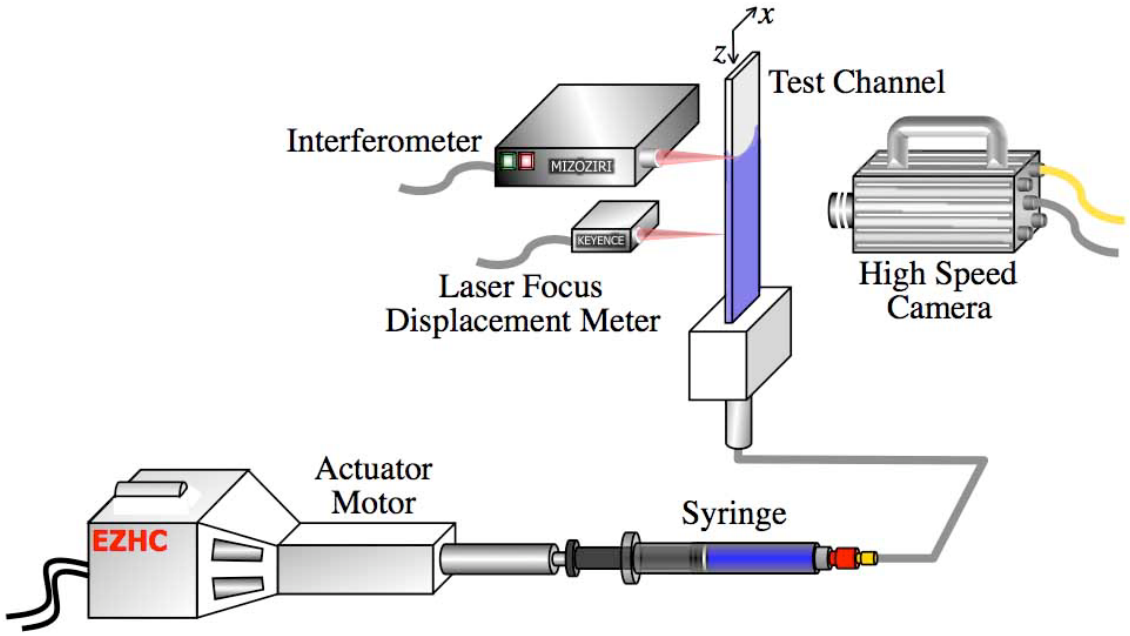

Fig. 1 Schematic diagram of the experimental setup.

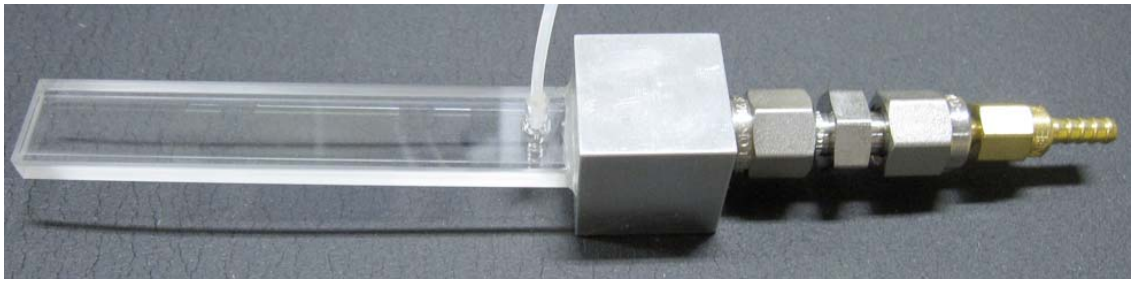

Fig. 2 Aluminum block connected to the high aspect ratio rectangular channel.

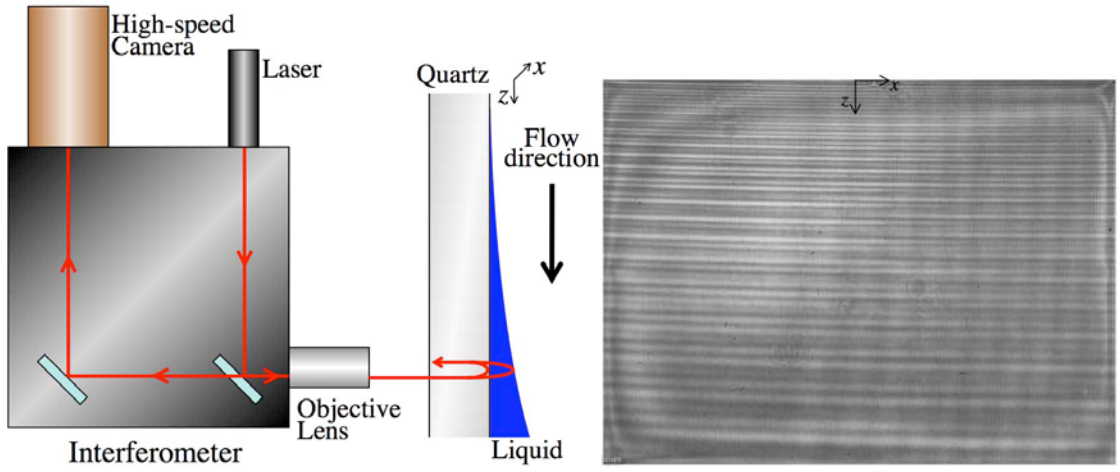

(a) (b)

Fig. 3 Principle of interferometer: (a) schematic diagram, (b) example of fringe pattern image.

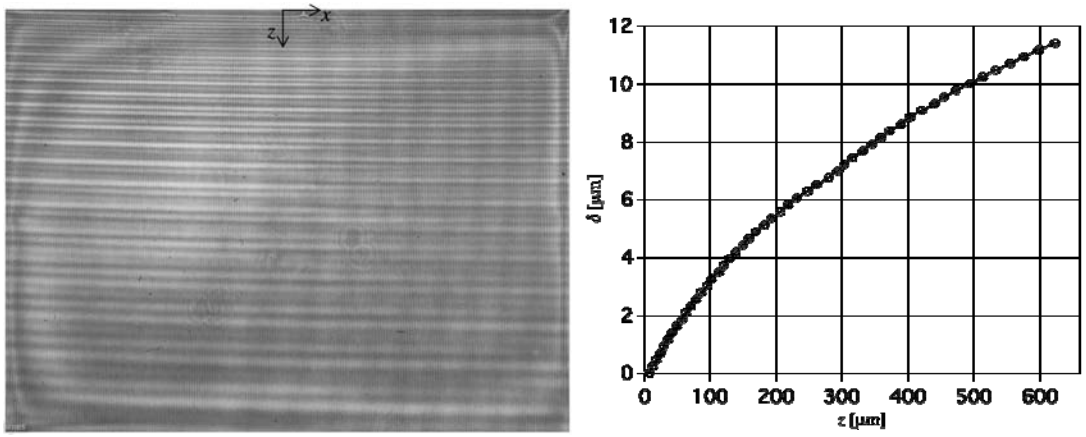

(a) (b)

Fig. 4 Profile of liquid film thickness along the flow direction (*z* axis): (a) captured fringe pattern image, (b) calculated liquid film thickness from the fringe pattern image.

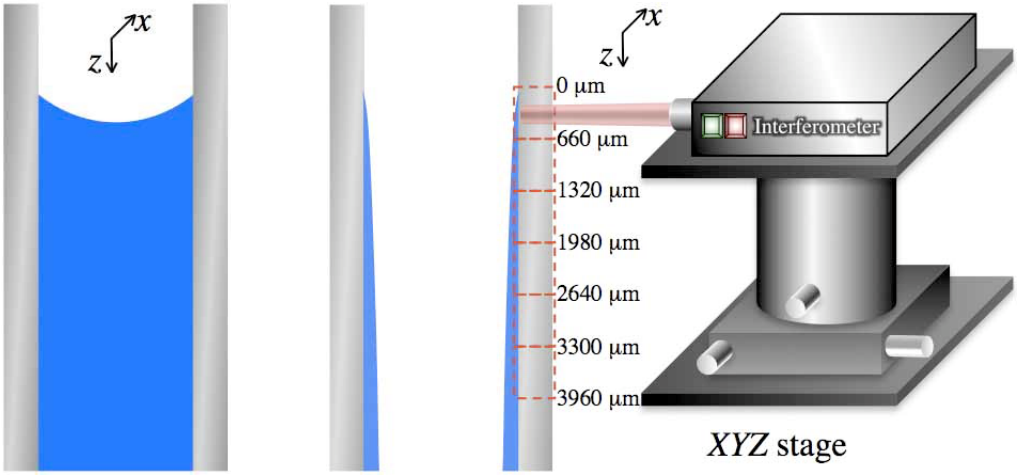

(a) Initial profile (b) After film formation

Fig. 5 Measurement positions for interferometer experiment.

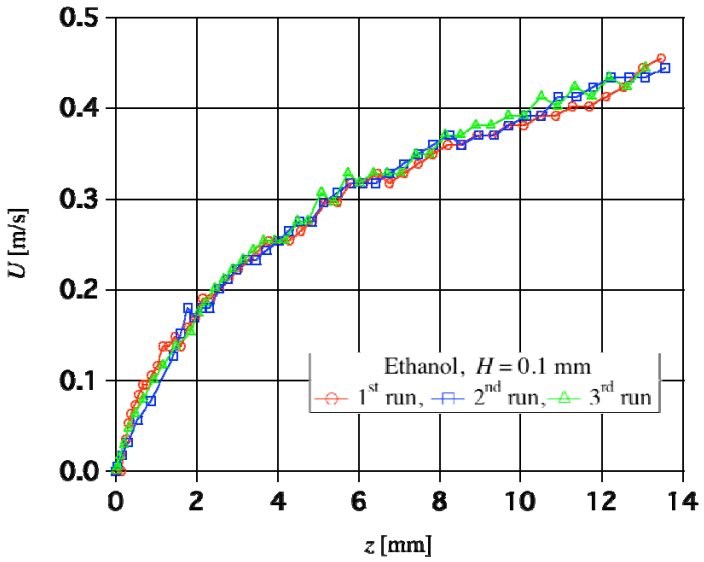

Fig. 6 Measured velocity variations along the flow direction.

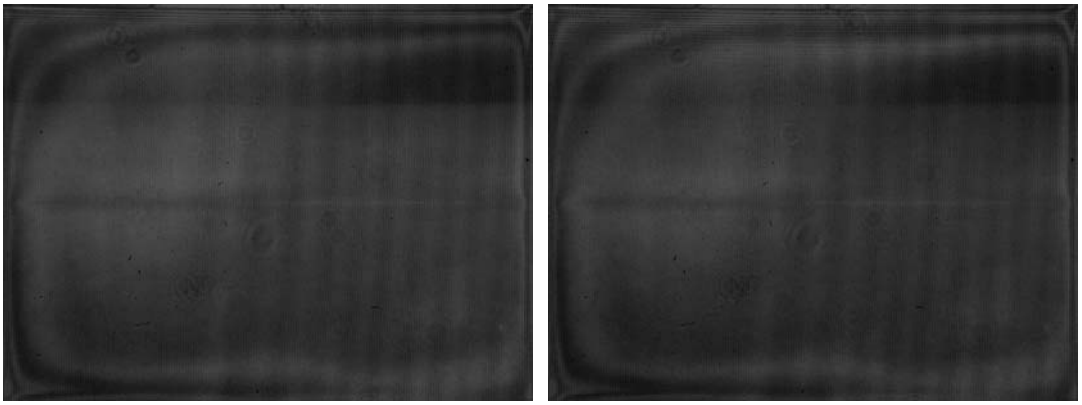

(a) t = 0 ms (b) t = 2 ms

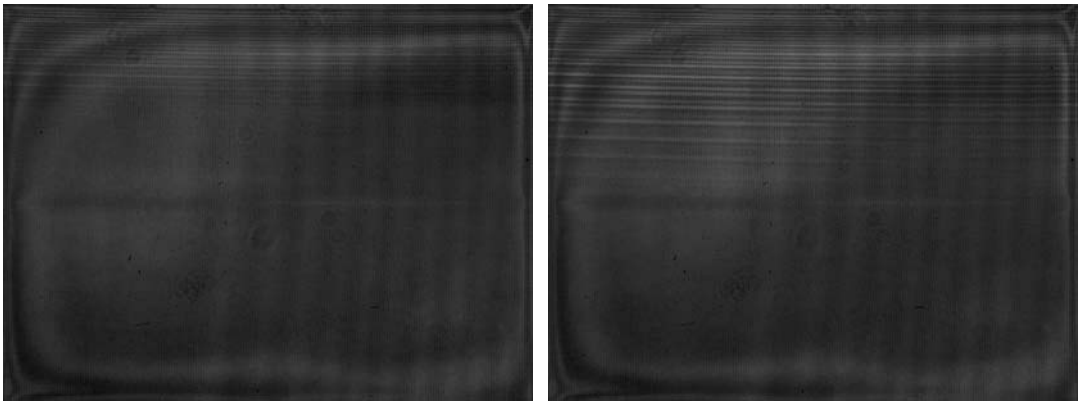

(c) t = 3 ms (d) t = 4 ms

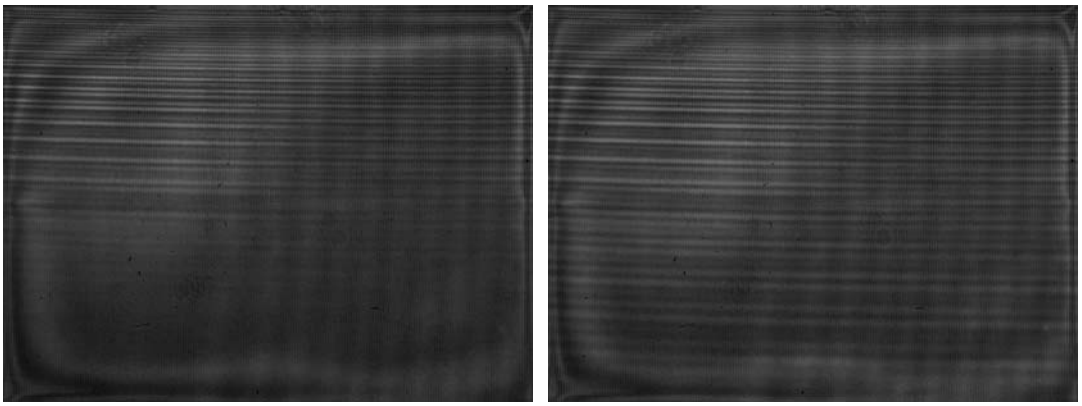

(e) t = 5 ms (f) t = 6 ms

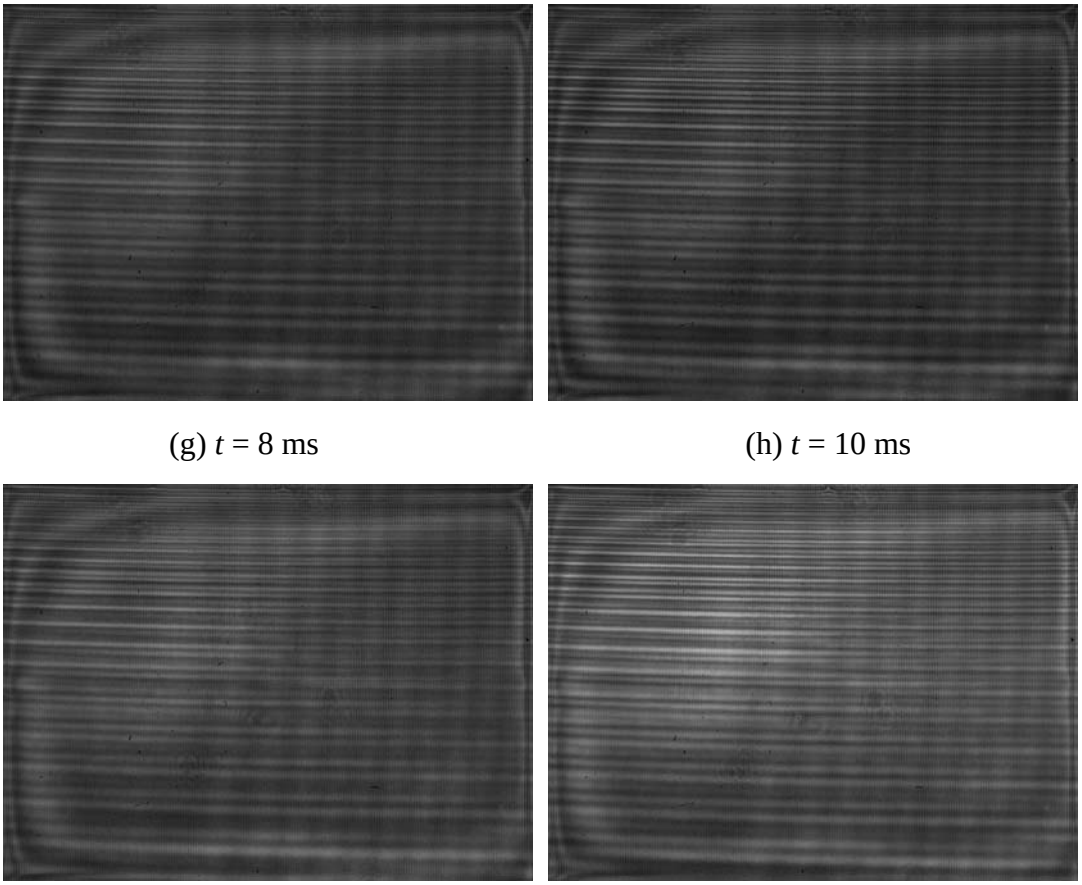

(g) t = 8 ms (h) t = 10 ms

(i) t = 15 ms (j) t = 20 ms

Fig. 7 Time variation of fringe pattern image at first position in Fig. 7 at (a) t = 0 ms, (b) t = 2 ms, (c) t = 3 ms, (d) t = 4 ms, (e) t = 5 ms, (f) t = 6 ms, (g) t = 8 ms, (h) t = 10 ms, (i) t = 15 ms, (j) t = 20 ms.

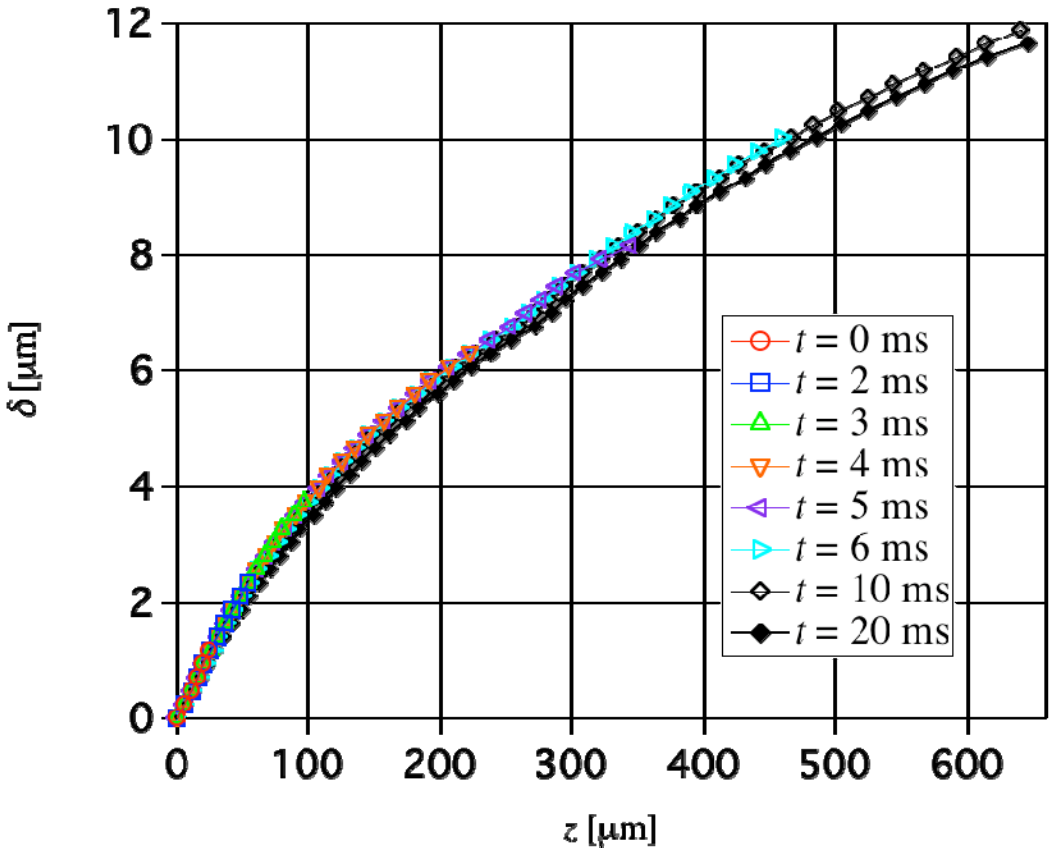

Fig. 8 Time variation of the liquid film profile.

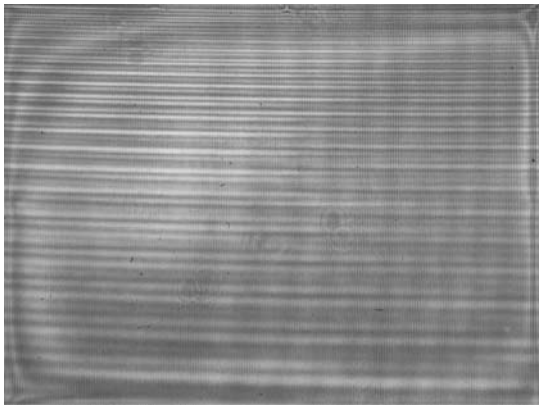

(a) z = 0 - 660 μm, 1st position

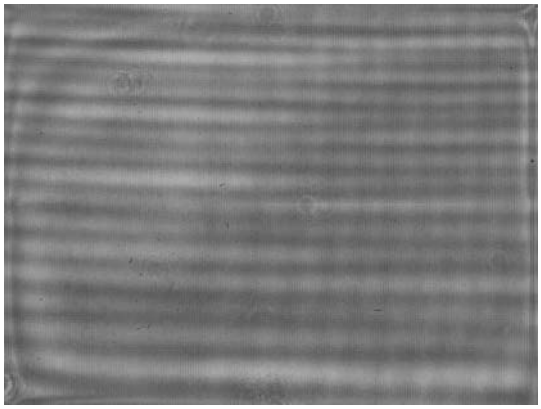

(b) z = 660 - 1320 μm, 2nd position

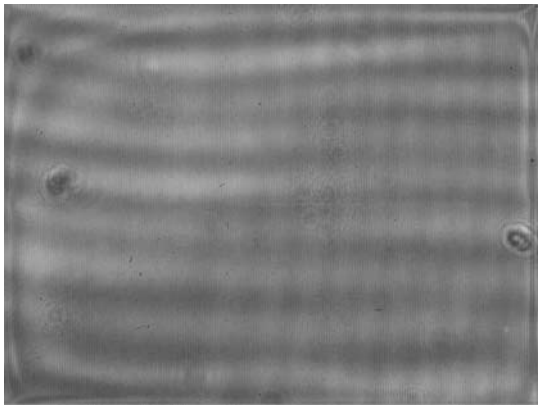

(c) z = 1320 - 1980 μm, 3rd position

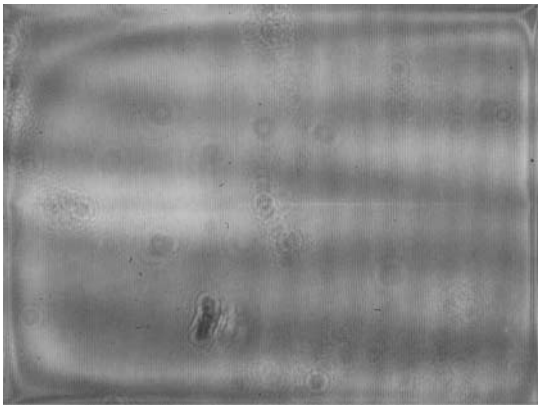

(d) z = 1980 - 2640 μm, 4th position

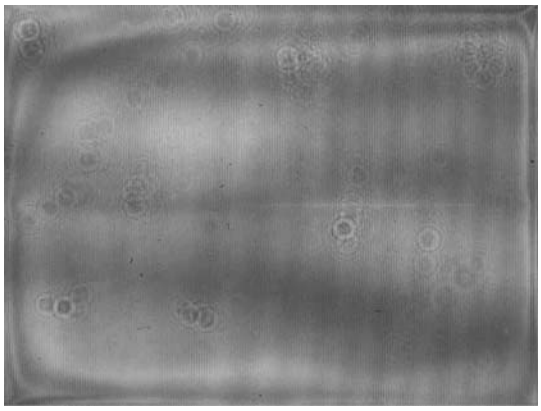

(e) z = 2640 - 3300 μm, 5th position

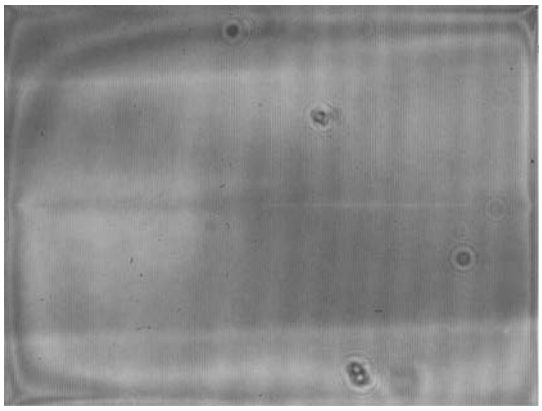

(f) z = 3300 - 3960 μm, 6th position

Fig. 9 Captured fringe pattern images along the flow direction: (a) z = 0 - 660 μm, 1st position, (b) z = 660 - 1320 μm, 2nd position, (c) z = 1320 - 1980 μm, 3rd position, (d) z = 1980 - 2640 μm, 4th position, (e) z = 2640 - 3300 μm, 5th position, (f) z = 3300 - 3960 μm, 6th position.

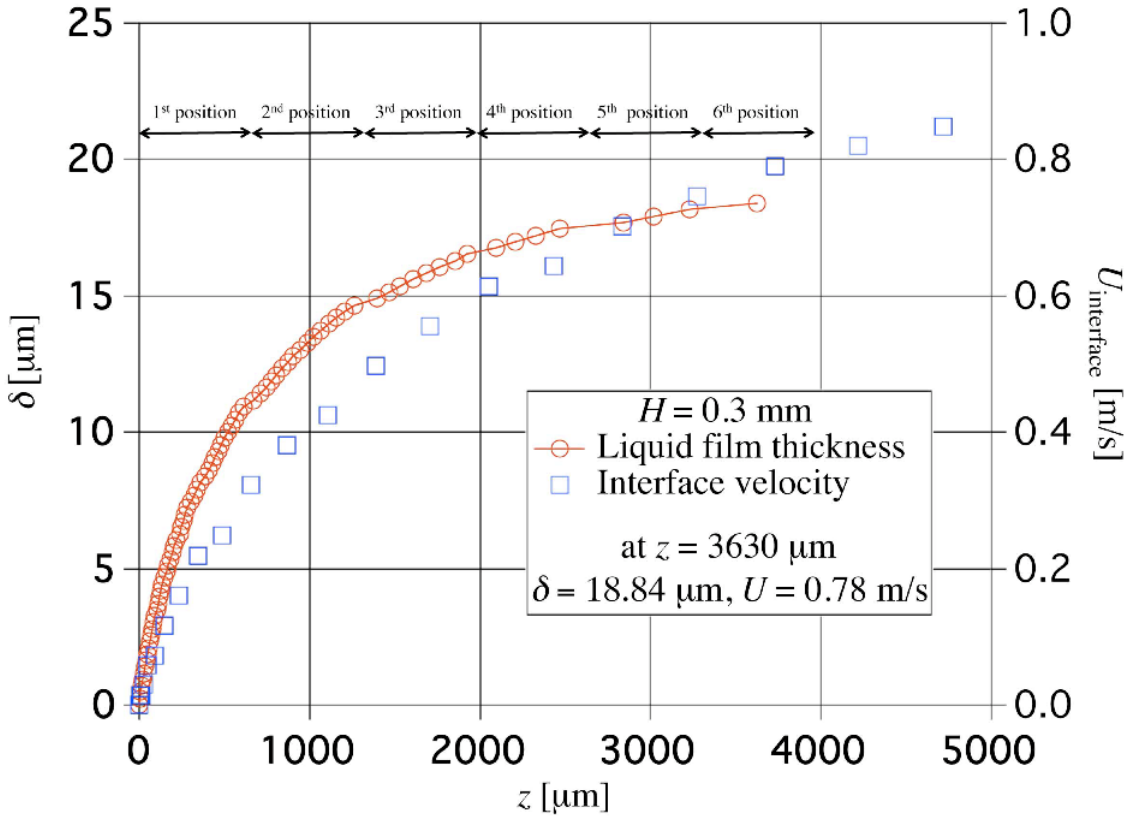

Fig. 10 Liquid film profile and interface velocity along the flow direction.

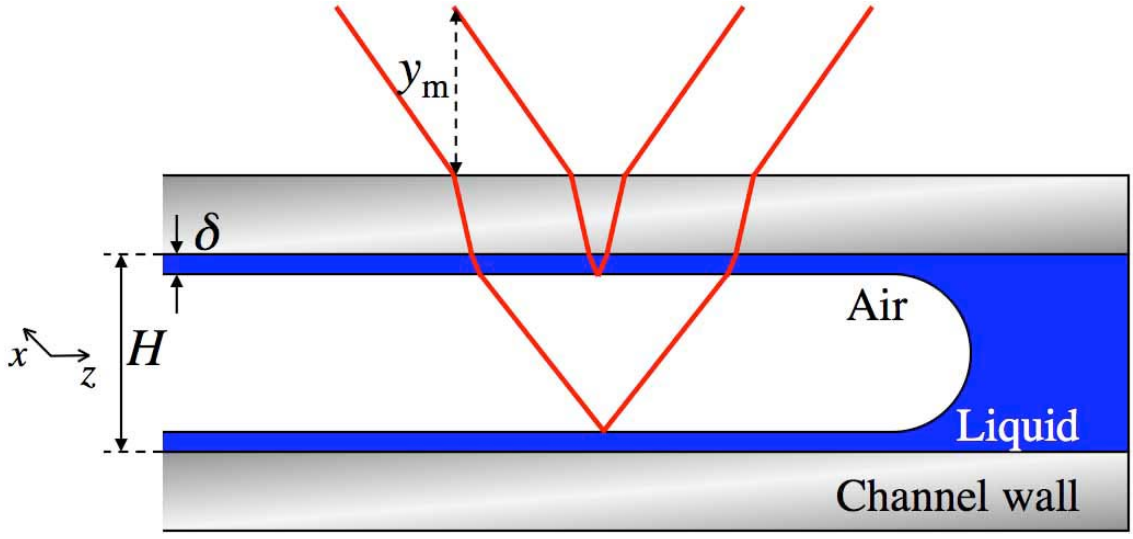

Fig. 11 Laser paths in a micro parallel channel.

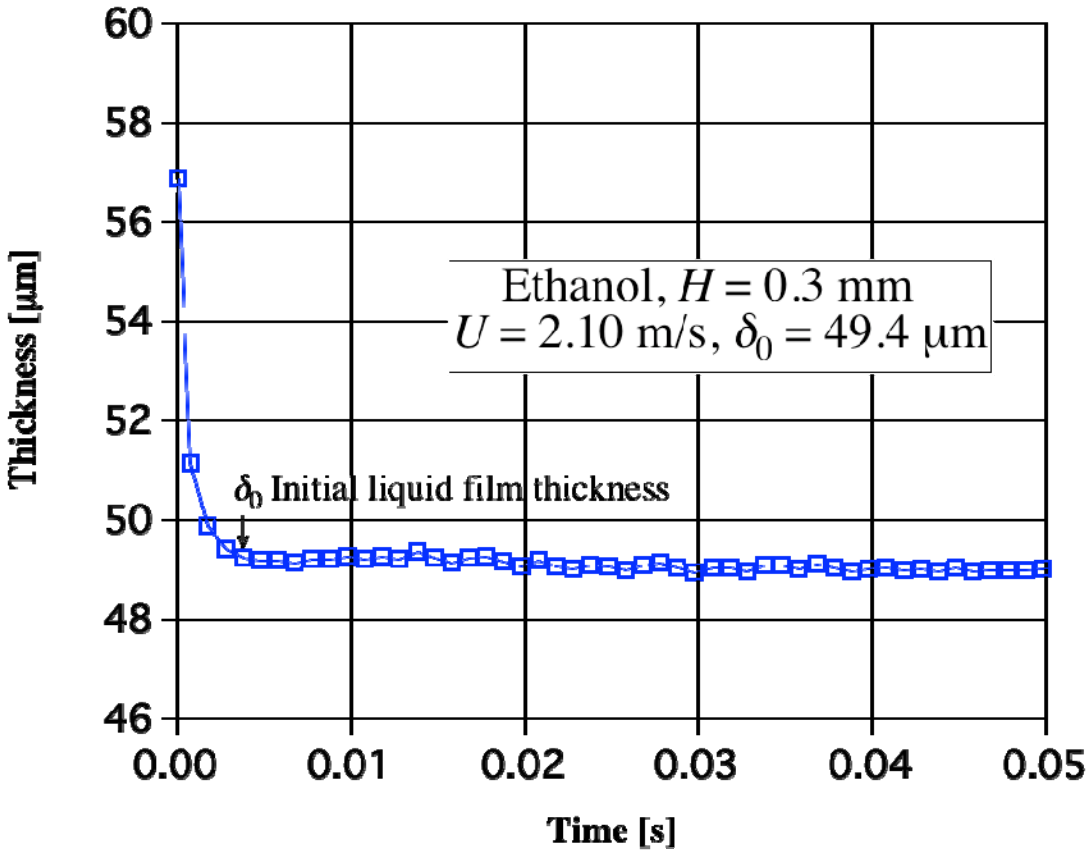

Fig. 12 Time variation of liquid film thickness measured by laser focus displacement meter.

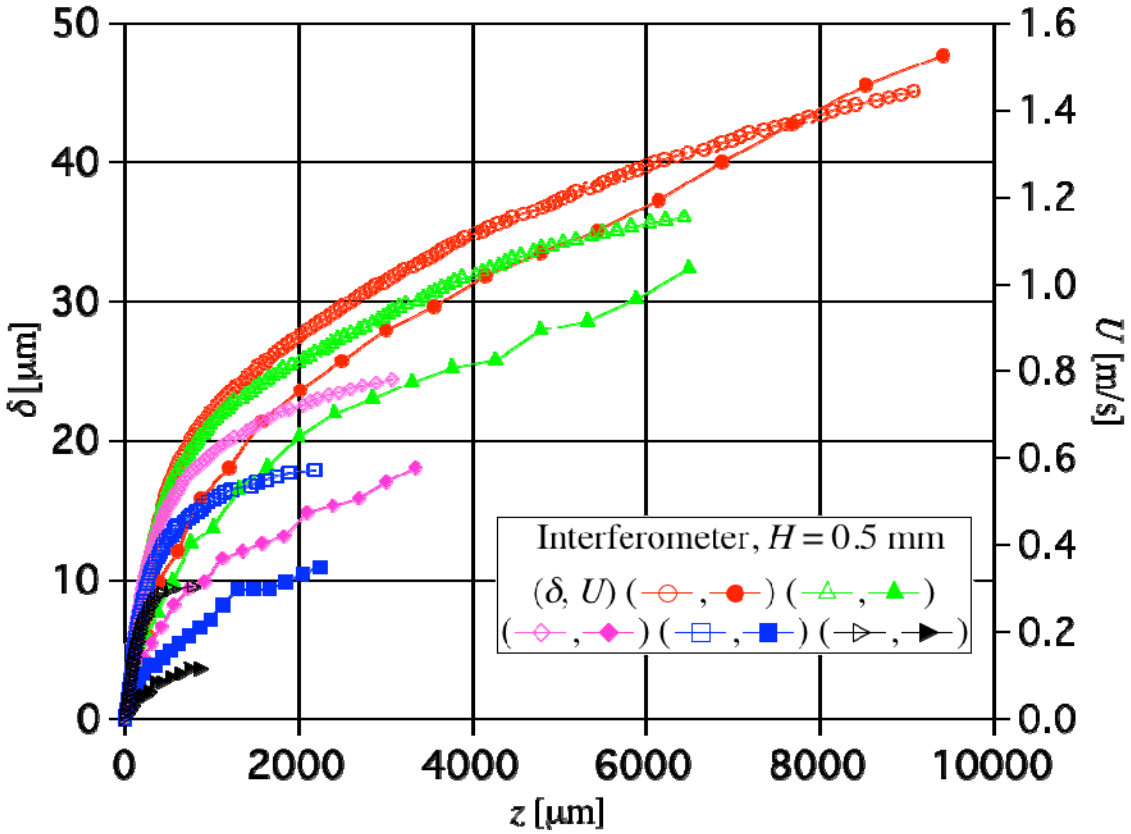

Fig. 13 Liquid film thickness and interface velocity along the flow direction, H = 0.5 mm.

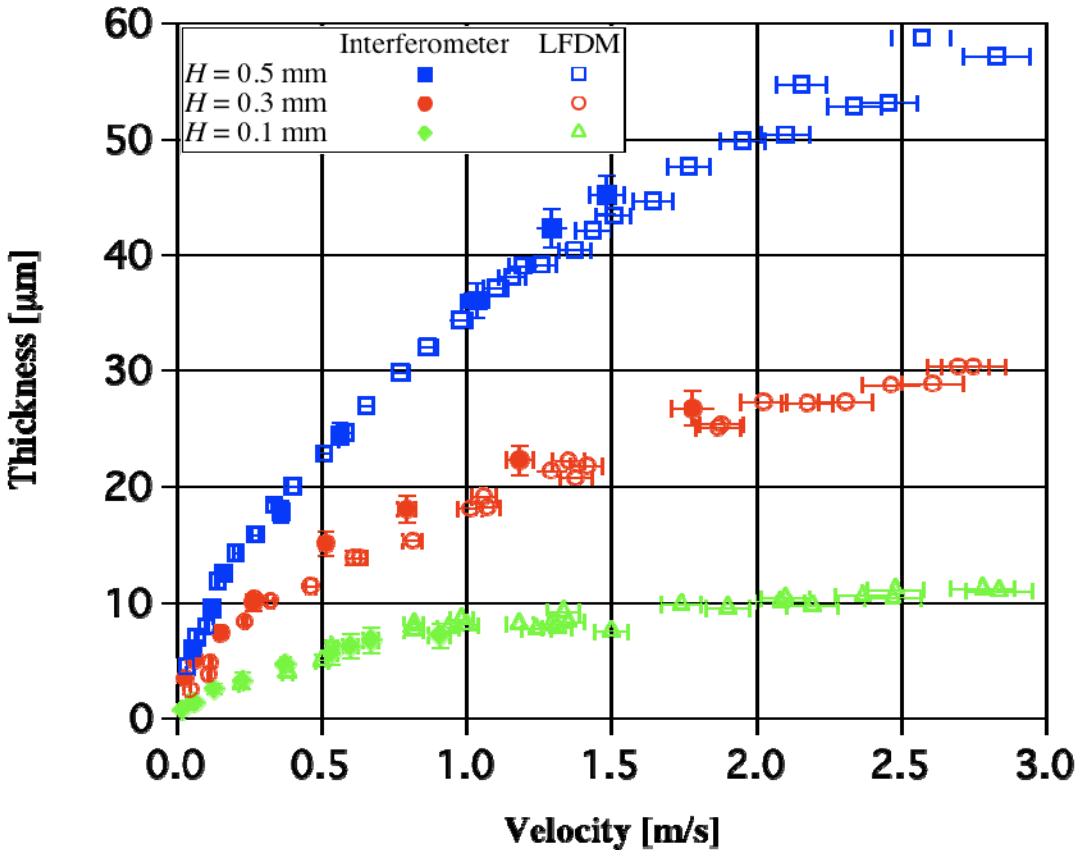

Fig. 14 Liquid film thicknesses measured by interferometer and LFDM versus interface velocities.

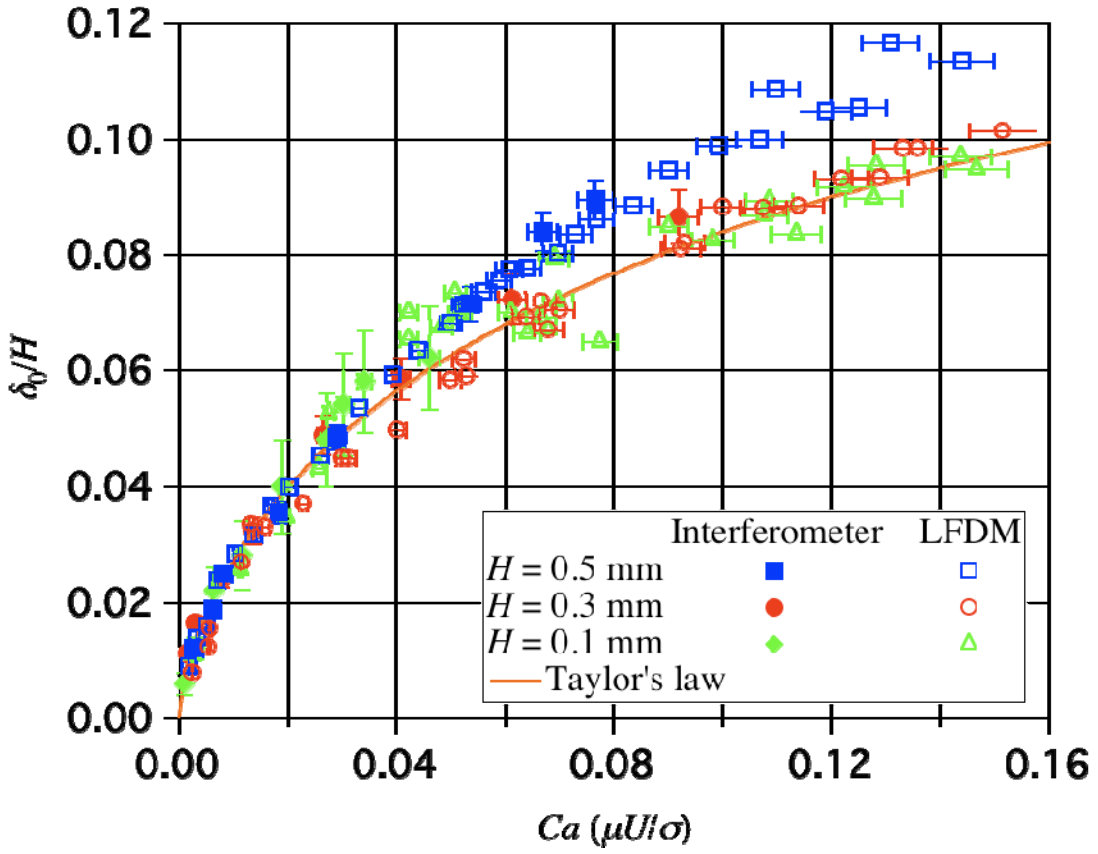

Fig. 15 Dimensionless liquid film thicknesses δ_0/H versus capillary number $Ca = \mu U/\sigma$.

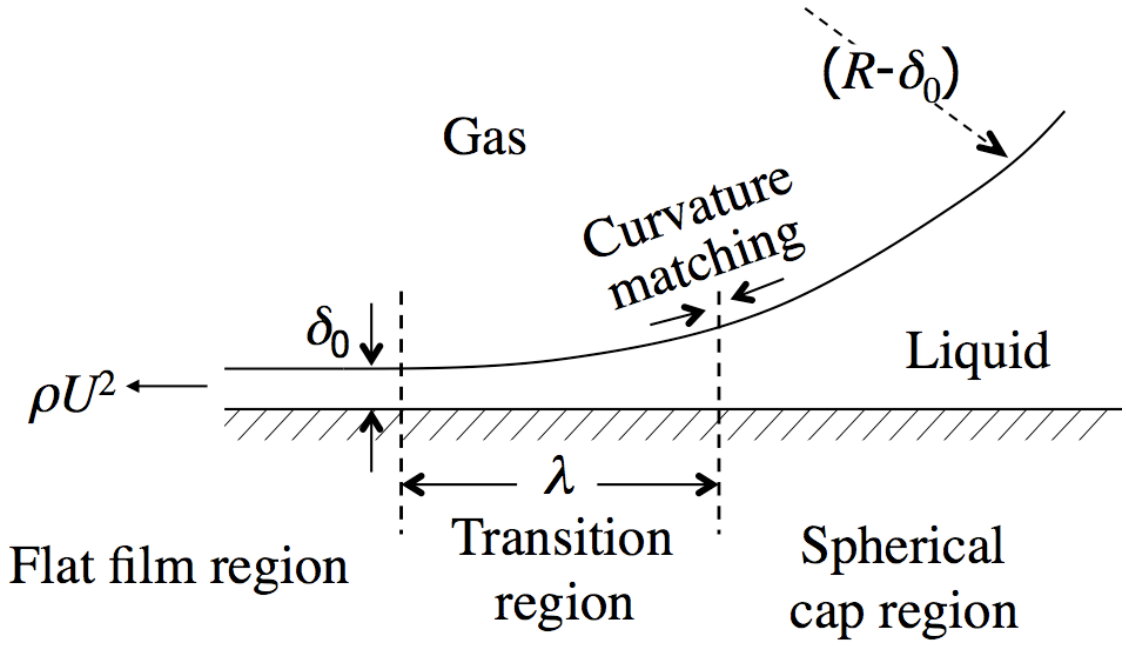

Fig. 16 Schematic diagram for the scaling analysis on the liquid film thickness in a micro tube (Han and Shikazono, 2009a).

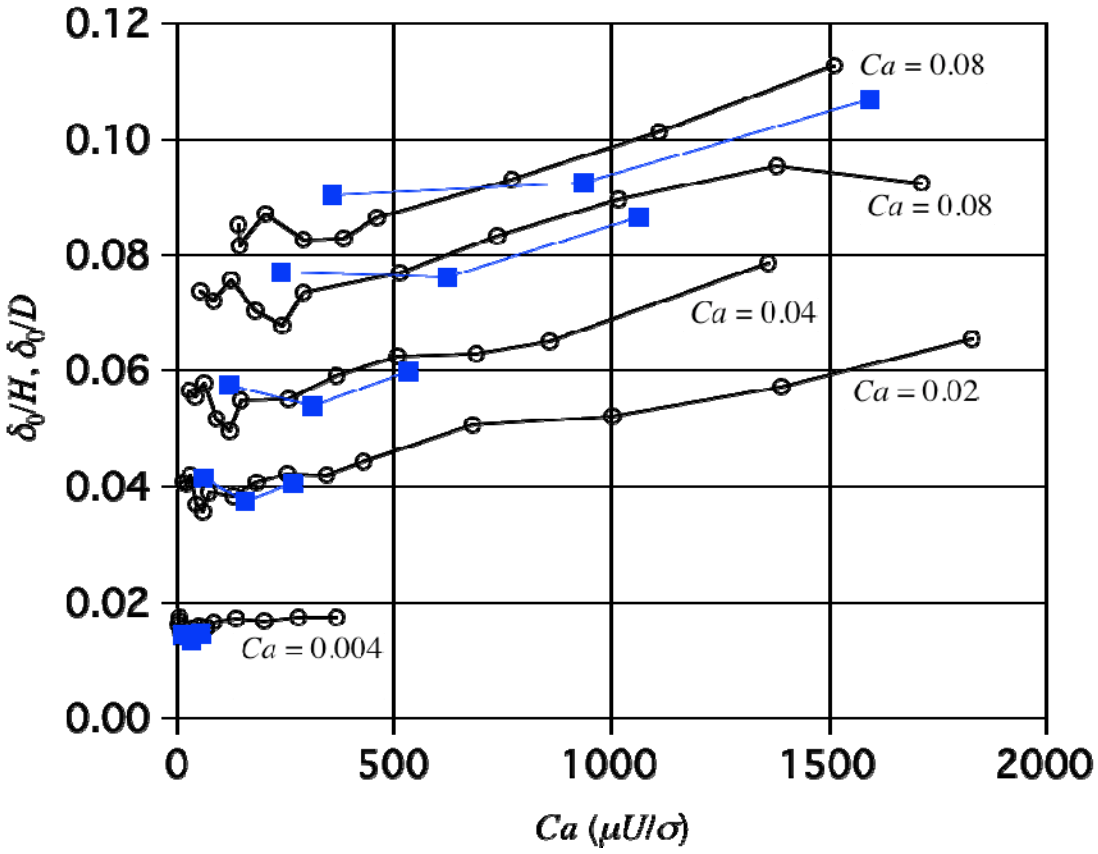

Fig. 17 Dimensionless liquid film thickness versus Reynolds number based on hydraulic diameter at fixed capillary numbers.

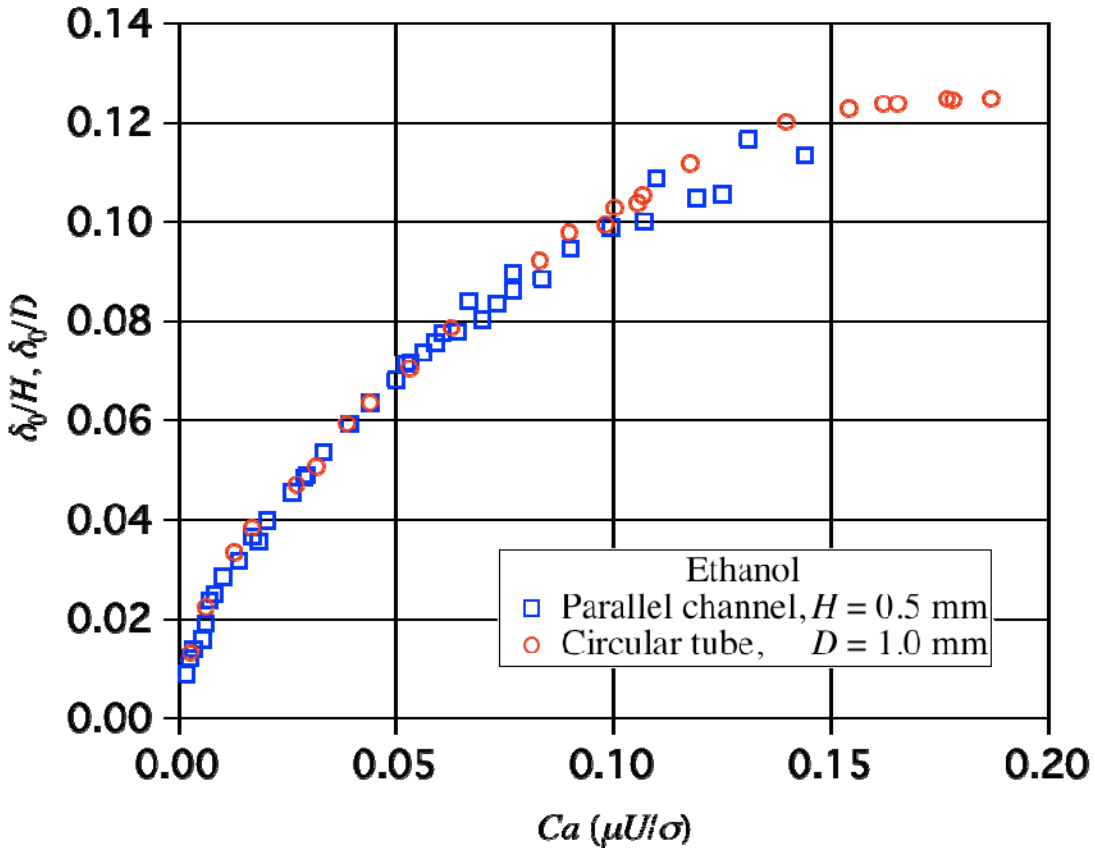

Fig. 18 Dimensionless liquid film thickness versus capillary number in the parallel channel of H = 0.5 mm and the circular tube of D = 1.0 mm

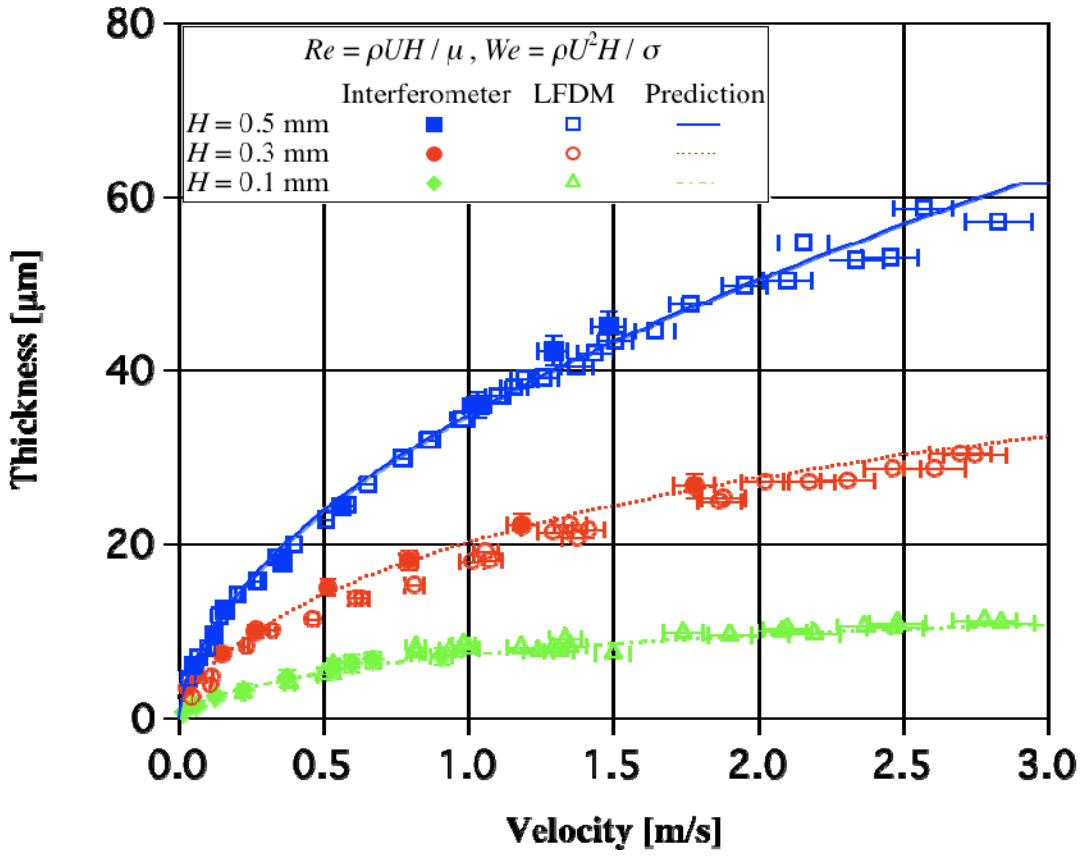

Fig. 19 Comparison between the measured liquid film thicknesses and the predicted values with Eq. (10) using hydraulic diameter as the characteristic length for *Re* and *We*.

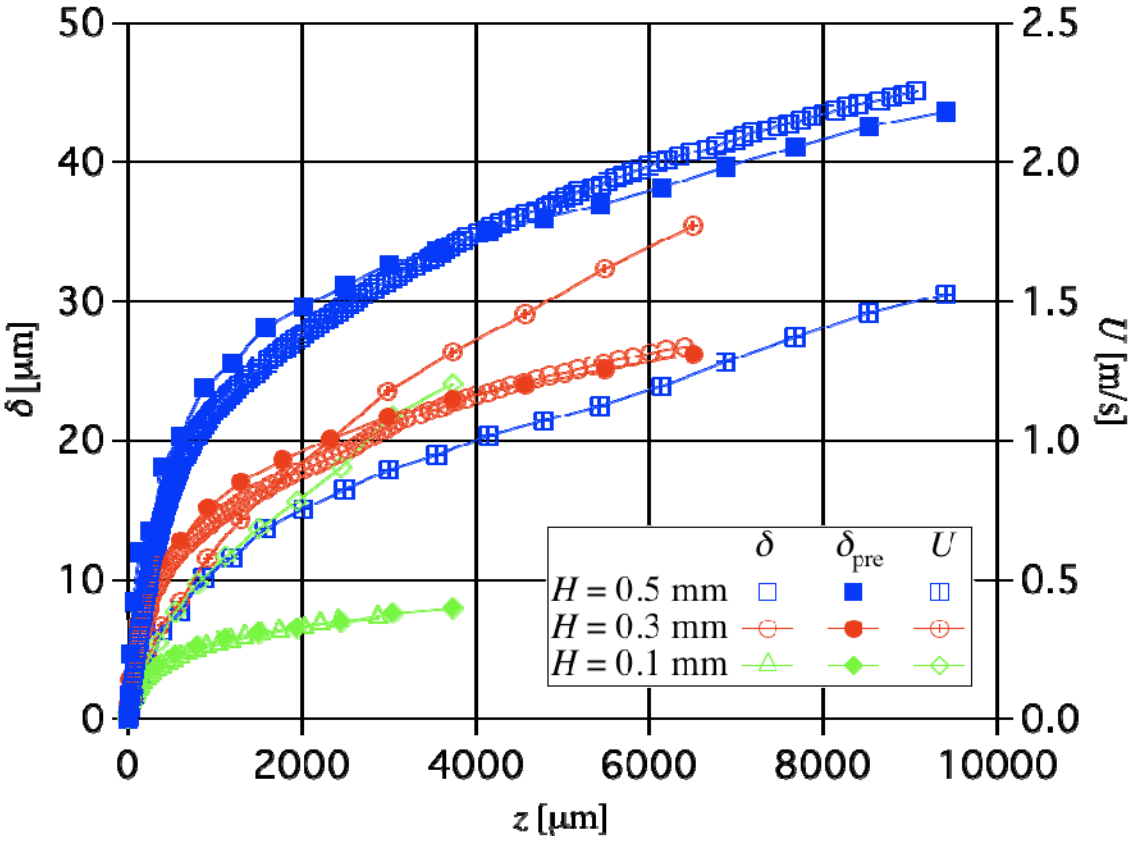

Fig. 20 Comparison between the liquid film profile obtained with interferometer and the predicted liquid film profile from interface velocity profile.

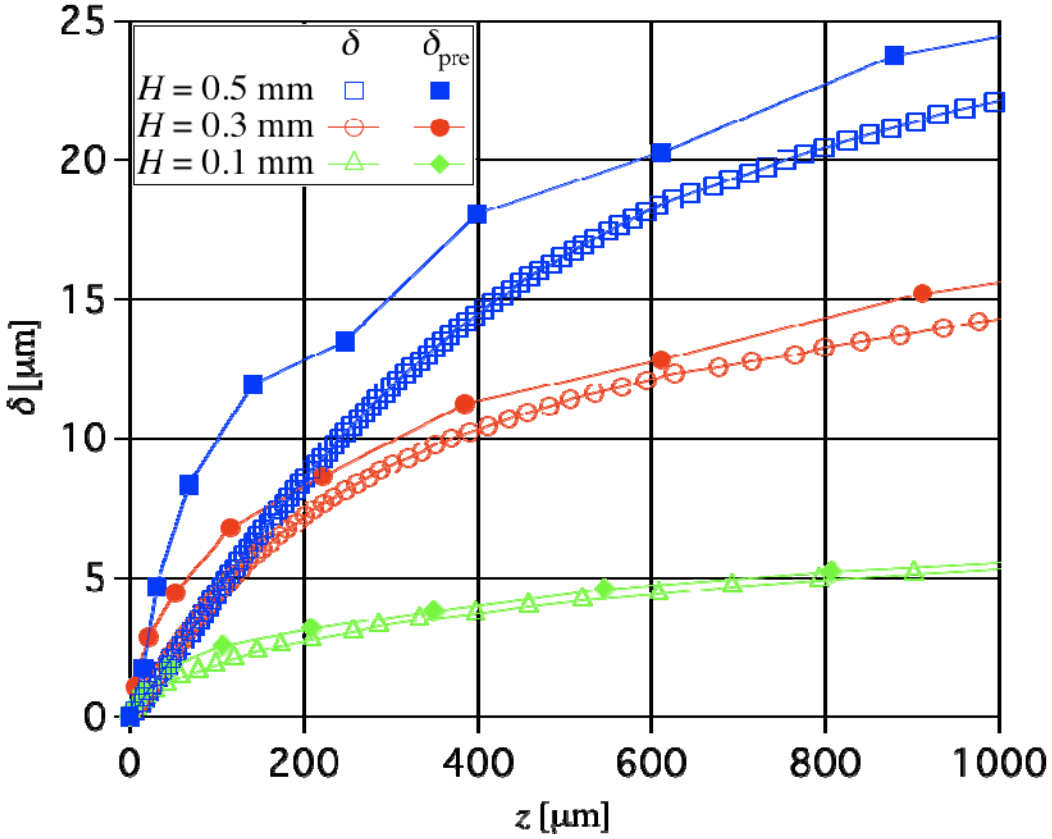

Fig. 21 Magnification of Fig. 20 very close to the initial gas-liquid interface position.